THE JOURNAL OF PHYSICAL CHEMISTRY C
A JOURNAL OF THE AMERICAN CHEMICAL SOCIETY

pubs.acs.org/JPCC

Article

Complexity of a Co_3O_4 System under Ambient-Pressure CO_2 Methanation: Influence of Bulk and Surface Properties on the Catalytic Performance

Anastasiia Efremova, T. Rajkumar, Ákos Szamosvölgyi, András Sápi,* Kornélia Baán, Imre Szenti, Juan Gómez-Pérez, Gábor Varga, János Kiss, Gyula Halasi, Ákos Kukovecz, and Zoltán Kónya

Cite This: *J. Phys. Chem. C* 2021, 125, 7130−7141

Read Online

ACCESS | Metrics & More | Article Recommendations | Supporting Information

ABSTRACT: Although using supported noble-metal catalysts for CO_2 hydrogenation is an effective solution due to their excellent catalytic properties, metal oxide supports themselves can exhibit good activity being more economically feasible. This work focuses on investigating the complexity of the Co_3O_4 system during the CO_2 methanation reaction, which is usually accompanied by the formation of unstable dispersions of cobalt oxide and metallic Co. Herein, we have tested different types of Co_3O_4: synthetically prepared mesoporous m-Co_3O_4 (BET surface area, 95 m^2/g) and commercial c-Co_3O_4 (BET surface area, 15 m^2/g; purchased from Merck) in the CO_2 methanation reaction under different reduction temperatures (273−673 K). The reduction temperature was adjusted to 573 K for both the catalysts to reach the optimal Co/cobalt oxide ratio and consequently the best catalytic performance. m-Co_3O_4 is more active (CO_2 conversion 95%) and stable at higher temperatures compared to c-Co_3O_4 (CO_2 conversion 63%) due to its morphology-induced ~66 times higher surface basicity. DRIFTS results showed differences in the detected surface species: formate was observed on m-Co_3O_4 and was proven to contribute to the total methane formation. It was revealed that in CO_2 methanation reaction, both bulk and surface properties such as morphology, cobalt oxidation states, acid−base properties, and presence of defect sites directly affect the catalytic performance and reaction mechanism. Furthermore, 1% 5 nm Pt nanoparticles were loaded onto the Co_3O_4s to check the competitiveness of the catalysts. This study evidences on a cheap noble-metal-free catalyst for CO_2 methanation consisting of m-Co_3O_4 with competitive activity and ~100% CH_4 selectivity.

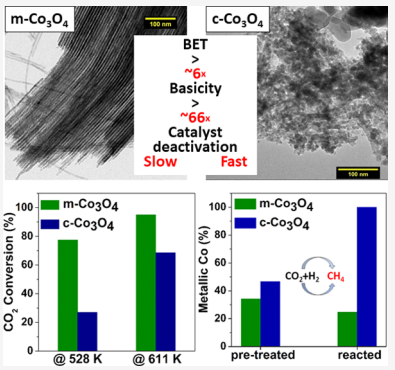

1. INTRODUCTION

One of the currently most important ecological concerns is associated with the growing concentration of CO_2 in the atmosphere, which occurs due to the intense utilization of carbon-rich fossil fuels such as coal, oil, and natural gas. The increase of atmospheric CO_2 contributes to a series of environmental problems such as global warming and ocean acidification.[1,2] Catalytic hydrogenation of CO_2 using a sustainable H_2 source not only reduces CO_2 emissions but also produces valuable fuels and chemicals.[3] However, CO_2 is a stable molecule that requires an energy-demanding catalyst for its activation.[4]

Recently, noble-metal−metal-oxide catalysts have received much attention owing to their extensive applications in CO_2 methanation.[5−7] In these systems, metal oxides not only aid for the dispersion of noble metals but also affect catalytic activities due to the presence of strong metal−support interaction.[8,9] However, noble metals are expensive materials; hence, the search for new solutions is of great interest nowadays.

The Co-based catalysts have been widely implemented for Fischer−Tropsch synthesis, methanol, and higher alcohol synthesis.[10] However, they proved to be particularly active and highly selective for the production of methane (Table S1). The methane and CO selectivity are determined by multiple factors such as CO_2 conversion, reduction temperature, reaction temperature, pressure, catalyst amount, and the structure of the support.[11]

The Co-based catalysts under CO_2 hydrogenation reaction is a complex dynamic system that often demonstrates the coexistence of different phases such as Co_3O_4, CoO, and Co on the surface of the catalyst. The composition of the phases and distribution between them are strongly influenced by the reduction temperature, structure, and morphology of the catalyst and directly affect the catalytic performance of the material (Table S1).

The focus of the present study lies in deriving the catalyst properties−performance correlations in the Co_3O_4 system. Herein, we compared different types of Co_3O_4 material during

Received: October 27, 2020
Revised: January 28, 2021
Published: February 10, 2021

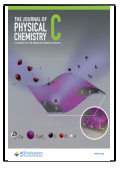

https://dx.doi.org/10.1021/acs.jpcc.0c09717
J. Phys. Chem. C 2021, 125, 7130−7141

CO_2 methanation at ambient pressure: mesoporous Co_3O_4 (further denoted as m-Co_3O_4) prepared by the hard template method and commercial Co_3O_4 (further denoted as c-Co_3O_4) purchased from Merck. The catalysts were tested at different reduction temperatures to elucidate the effect of cobalt oxide states on catalytic performance. A short discussion on the role of formed phases and plausible reaction mechanism is carried out. m-Co_3O_4 is shown to have good and stable catalytic activity in CO_2 methanation reaction compared to its noble-metal-loaded counterpart and other Co-based catalysts.

2. EXPERIMENTAL SECTION

2.1. Chemicals. Pluronic-123 (average $M_n \sim 5800$) and tetraethyl orthosilicate (98%) were purchased from Sigma-Aldrich. $H_2PtCl_6{\cdot}6H_2O$ and *n*-butanol (99.5%) were obtained from Reanal Labor. Poly(vinylpyrrolidone) (average molecular weight ~ 40 000) was purchased from BASF. $Co(NO_3)_2{\cdot}6H_2O$ (99%) was purchased from Spektrum-3D. Co_3O_4 was purchased from Merck. Ethylene glycol (99.7%), NaOH (99.95%), HCl (37%), toluene (99.98%), *n*-hexane (98.54%), ethanol (99.94%), and acetone (99.96%) were purchased from Molar Chemicals. All of the chemicals were used as received without further purification.

2.2. Synthesis of 5 nm Pt Nanoparticles. $H_2PtCl_6{\cdot}6H_2O$ (50 mg) and PVP (220 mg) were dissolved in 10 mL of ethylene glycol, separately. The solutions were mixed in a 25 mL round-bottom flask and refluxed at 433 K for 60 min under argon purging. The Pt nanoparticles were collected by precipitation with 40 mL of acetone, followed by several washing cycles based on ethanol dispersion and hexane precipitation. The product was finally redispersed in 10 mL of ethanol.

2.3. Synthesis of Mesoporous Cobalt Oxide. For the preparation of mesoporous cobalt oxide support (m-Co_3O_4), KIT-6 silica was used as a template.[12] In a typical synthesis, 4.65 g of $Co(NO_3)_2{\cdot}6H_2O$ was dissolved in 8 mL of water and mixed with a suspension of 4 g of KIT-6 in 50 mL of toluene. Vigorous stirring was applied to the mixture at 338 K until the total evaporation of toluene. After the evaporation, the precipitated product was collected and dried at 333 K overnight, followed by calcination at 573 K for 6 h. The silica template was completely removed by several washing steps using 2 M aqueous NaOH solution. The filtered product was dried at 332 K overnight.

2.4. Synthesis of Mesoporous Cobalt Oxide-Supported Pt Catalysts. To fabricate supported catalysts, the ethanol suspension of Pt nanoparticles and m-Co_3O_4 were mixed in ethanol and sonicated in an ultrasonic bath (40 kHz, 80 W) for 3 h. The supported nanoparticles were collected by centrifugation. The products were washed with ethanol three times before they were dried at 353 K overnight.

2.5. Powder X-ray Diffraction (XRD). XRD studies of the samples were performed on a Rigaku MiniFlex II instrument with a Ni-filtered Cu Kα source in the range of $2\theta = 10-80°$. For the measurements under inert atmosphere (N_2), a PW 1830 diffractometer (Philips) using Cu Kα radiation (λ = 0.1542 nm) and operated in Bragg–Brentano geometry with a Ni filter at a voltage of 40 kV and a current of 30 mA was used.

2.6. Hydrogenation of Carbon Dioxide in a Continuous-Flow Reactor. The catalytic reactions were carried out at 1 atm pressure in a fixed-bed, continuous-flow reactor (8 mm i.d.) made from quartz. The dead volume of the reactor was filled with quartz beads. The operating temperature was controlled by a thermocouple placed inside an oven close to the reactor wall. For catalytic studies, small fragments (about 1 mm) of slightly compressed pellets were used. Typically, the reactor filling contained 200 mg of catalyst. In the reacting gas mixture, the CO_2/H_2 molar ratio was 1:4. The CO_2/H_2 mixture was introduced to the reactor with mass flow controllers (Aalborg), and the total flow rate was 50 mL·min^{-1}. The reacting gas mixture flow entered and left the reactor through an externally heated tube to avoid condensation. Analysis of the gases was performed with an Agilent 4890 gas chromatograph using Equity-1 capillary and Porapak QS packed columns to allow the complete separation of the reactants and products. The gases were detected simultaneously by thermal conductivity and flame ionization detectors. Before the catalytic experiments, the as-received catalysts were oxidized in the O_2 atmosphere at 573 K for 30 min and thereafter were reduced in H_2 at 273–673 K for 60 min.

2.7. X-ray Photoelectron Spectroscopy (XPS). For XPS analysis, a powder sample was pressed into a tablet with ca. 1 cm diameter and a few millimeters thickness. Pretreatment (in O_2 at 573 K for 30 min; in H_2 at 573 K for 60 min) and ex situ sample preparations were carried out in the modified prechamber of a Kratos Analytical XSAM800 instrument. After that, the samples were introduced into the main chamber to register spectra. After data acquisition, CO_2 and H_2 (1:4 ratio) were introduced to the prechamber, and the reaction time was 30 min at 673 K and 1 atm. Then, the spectra were collected once again.

The XP spectra were obtained with a nonmonochromatized Mg Kα X-ray source (1253.6 eV). The X-ray gun was operated at 144 W (12 kV, 12 mA) for both survey and high-resolution spectra. The survey spectra were collected at an 80 eV pass energy with a step rate of 1 point per eV. The high-resolution spectra were collected at a pass energy of 40 eV with a 0.1 eV energy resolution. All high-resolution spectra were charge-corrected for the aliphatic component of the C 1s spectrum region having a peak maximum at 284.8 eV. For background correction, a standard Shirley background was applied in all cases.

2.8. In Situ Diffuse Reflectance Infrared Fourier Transform Spectroscopy (DRIFTS). The DRIFTS analyses were carried out in an "Agilent Cary-670" FTIR spectrometer equipped with "Harrick Praying Mantis" diffuse reflectance attachment. The sample holder contained two BaF_2 windows in the infrared path. The sample was pretreated as described above, cooled down to room temperature under helium flow, and the background spectrum was registered. At room temperature, a CO_2/H_2 mixture (1:4 molar ratio) and He stream with a total flow rate of 40 mL·min^{-1} were fed into the DRIFTS cell. The tubes were externally heated to avoid condensation. The catalyst was heated under the reaction feed linearly from room temperature to 673 K, with a heating rate of 20 K·min^{-1}, and IR spectra were collected at 50 K intervals. All spectra were recorded between 4000 and 900 cm^{-1} at a resolution of 2 cm^{-1}. Typically, 32 scans were registered. Due to the short optical path within the DRIFTS cell, the contribution of the reactant gases was negligibly small, and from gas-phase products, only the most intense features were observable.

2.9. Transmission Electron Microscopy (TEM). High-precision images of ultrathin samples of the catalysts were provided by an FEI TECNAI G2 20 X-Twin high-resolution

https://dx.doi.org/10.1021/acs.jpcc.0c09717
J. Phys. Chem. C 2021, 125, 7130–7141

transmission electron microscope (equipped with electron diffraction) operating at an accelerating voltage of 200 kV. The samples were presented on a copper grid-type holder coated with a thin layer of carbon.

2.10. Raman Spectroscopy. Raman characterization was performed with a 785 nm excitation wavelength in a Bruker Senterra II instrument. All of the samples were tested at a low nominal power of 1 mW with 30 s integration time. The in situ Raman spectra were collected in a temperature-controlled stage (Linkam, HFS600E), where the atmosphere was controlled by mass flow controllers (Aalborg) to reproduce the pretreatment conditions in the catalytic tests.

2.11. CO_2 Temperature-Programmed Desorption (CO_2-TPD). The temperature-programmed desorption (TPD) was carried out in a BELCAT-A apparatus using a reactor (quartz tube with 9 mm outer diameter) that was externally heated. Before the measurements, the catalyst samples were pretreated as described above. Thereafter, the sample was cooled in flowing He to 323 K and equilibrated for 15 min. The samples were flushed with CO_2 for 30 min and then flushed with He for 15 min at 323 K. The reactor was heated linearly at a rate of 10 K·min^{-1} up to 800 K. The CO_2 consumption was detected by a thermal conductivity detector (TCD).

3. RESULTS AND DISCUSSION

3.1. Characterization of the Catalysts. The morphology of Co_3O_4 samples was studied by transmission electron microscopy (TEM). The TEM image of the m-Co_3O_4 produced by the template method shows a regular, ordered structure with nanorod morphology. The average diameter of a nanorod is 5 nm (Figure 1a). The material has a specific

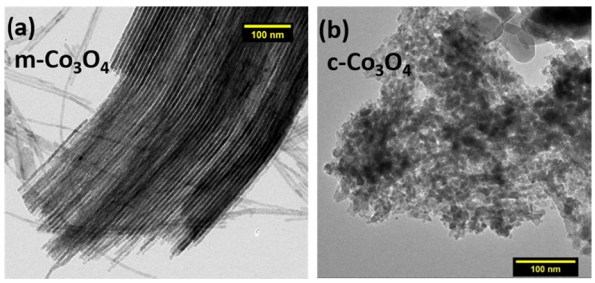

Figure 1. TEM images of (a) m-Co_3O_4 and (b) c-Co_3O_4.

surface area of 95 m^2/g and a typical pore volume of 34.4 Å. In contrast, c-Co_3O_4 support has no regular shape (Figure 1b) with a low specific surface area (Table 1).

Chemical characterization of the surface was carried out by means of CO_2 temperature-programmed desorption (CO_2-TPD), which was applied to identify the number of basic sites present on pretreated catalysts (Table 1). Obviously, the peak area of basic sites for m-Co_3O_4 is considerably higher compared to that of c-Co_3O_4, indicating that CO_2 adsorption

Table 1. Textural Properties and Basic Sites of the Catalysts

catalyst	BET surface (m^2/g)	pore radius (Å)	total pore volume (cm^3/g)	the number of basic sites (mmol CO_2/g)
m-Co_3O_4	95	34.4	0.153	0.6
c-Co_3O_4	15	24.6	0.042	0.009

was facilitated in the case of m-Co_3O_4. The increase in basic sites was mostly observable in the ca. 373−513 K temperature region, which corresponds to the enhancement of weak basic sites such as OH groups.[13] The enhanced surface basicity in the case of m-Co_3O_4 may arise due to the hard template synthesis method, aimed at producing ordered mesoporous structures. The applied reaction conditions initiated the generation of hydroxyl group-based vacancies having basic character.[14] In parallel with the appearance of these hydroxyl groups, the surface basicity is significantly enhanced in an exponential manner. It is generally accepted that the higher surface basicity is beneficial for the activation of CO_2 molecules.[15]

Being a reducible oxide, Co_3O_4 in a reducing environment forms metallic Co, which has strong hydrogenation ability and lacks RWGS activity.[16] The distribution of species on the surface and hence the catalytic activity are known to be heavily dependent on pretreatment conditions and reduction temperatures, in particular.[17] Hydrogen temperature-programmed reduction (H_2-TPR) experiments revealed that m-Co_3O_4 and c-Co_3O_4 are reduced to different extents from 473 to 673 K, meaning that the support morphology influences its redox behavior and c-Co_3O_4 can be reduced much easily (Figure S1). The same effect was reported earlier.[16]

Therefore, in the first experiment, the reduction temperatures varied in this temperature range to determine the optimal interphase. The pretreatment conditions were as follows: oxidation in O_2 for 30 min at 573 K and subsequent reduction in H_2 for 60 min from 273 (no reduction) to 673 K.

3.2. Effect of Reduction Temperatures. *3.2.1. X-ray Diffraction (XRD).* Figure 2 shows the XRD patterns of original m-Co_3O_4 and c-Co_3O_4 as well as their reduced samples. The m-Co_3O_4 exhibits peaks at 2θ = 31.3, 36.9, 38.6, 44.8, 55.7, 59.4, 65.35, and 77.3°, which correspond to crystal planes of (220), (311), (222), (400), (422), (511), (440), and (533) for Co_3O_4 cubic spinel structure (JCPDS card no. 43-1003)[18] (Figure 2a). However, c-Co_3O_4 shows additional XRD peaks apart from Co_3O_4 phase at 2θ = 36.6, 42.6, 61.7, and 77.6° assigned to the (111), (200), (220), and (222) planes of the cubic CoO, respectively (JCPDF no. 43-1004)[19] (Figure 2b). The oxidized Co_3O_4 samples (no reduction) showed only reflections of the Co_3O_4 cubic spinel structure. Since there is a CoO phase present in the original c-Co_3O_4, it is reduced easier—already at 473 K, while in the case of m-Co_3O_4, at this reduction temperature, only one phase of cubic Co_3O_4 with reduced intensities could be detected. Increasing the reduction temperature to 573 K results in the emergence of the CoO phase for m-Co_3O_4 as well. Furthermore, in both the cases, diffraction peaks at 2θ = 44.5 (111 crystal plane) and 76.1° (220 crystal plane) indicate the presence of the small amount of cobalt fcc (JCPDS no. 15-0806).[20] At the highest reduction temperature of 673 K, the catalysts consisted of primarily metallic cobalt (fcc), evidenced from diffraction peaks at 2θ = 44.5, 51.5 (200 crystal plane), and 76.1°; however, CoO phase was also registered for both the samples.

3.2.2. Catalytic Activity Tests. The catalytic performance of Co_3O_4 catalysts, reduced at different temperatures, was evaluated for CO_2 hydrogenation reaction in the 473−673 K temperature range and at 1 atm pressure. The CO_2 conversion is shown in Figure 3, while the maximum CO_2 consumption rate values are summarized in Table S2. m-Co_3O_4, reduced at 273 and 473 K, is inactive up to 550 K (Figure 3a). This may be attributed to the presence of only Co_3O_4 single phase,

https://dx.doi.org/10.1021/acs.jpcc.0c09717
J. Phys. Chem. C 2021, 125, 7130−7141

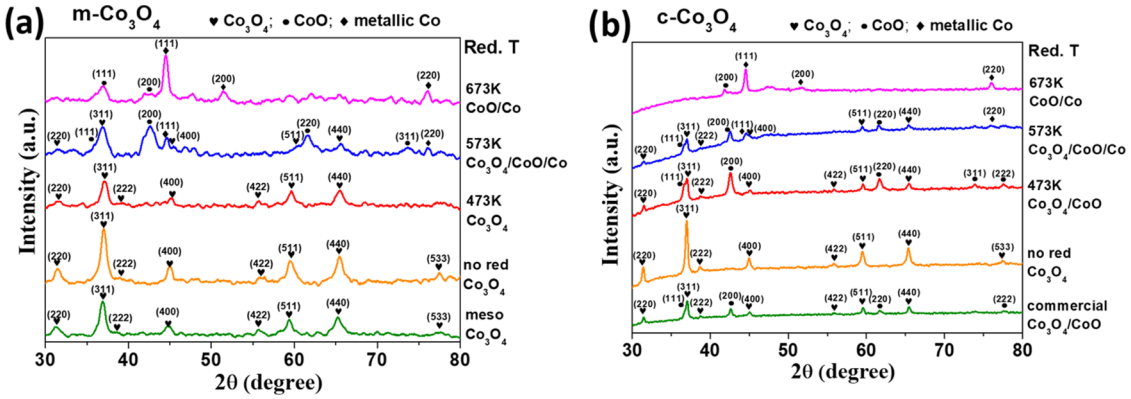

Figure 2. XRD patterns of (a) m-Co_3O_4 and (b) c-Co_3O_4 reduced at 273, 473, 573, and 673 K.

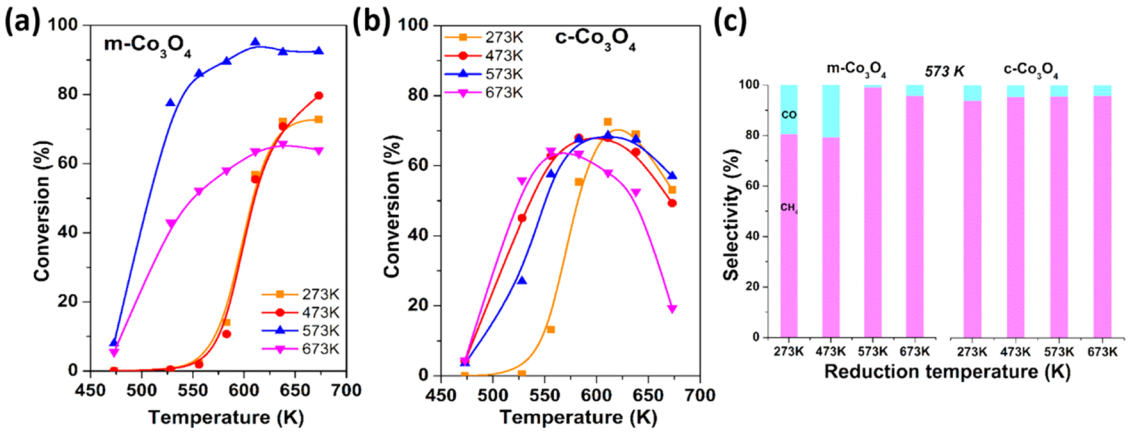

Figure 3. CO_2 conversion over (a) m-Co_3O_4 and (b) c-Co_3O_4 reduced at 273, 473, 573, and 673 K and (c) their CH_4 selectivity at 573 K.

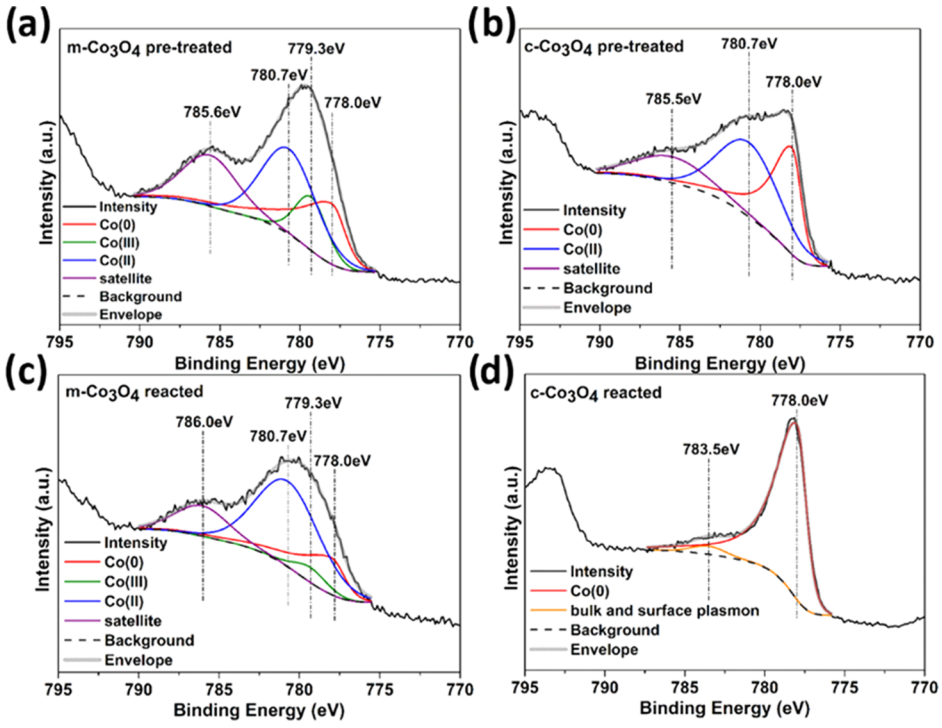

Figure 4. XPS spectra of Co 2p of the (a) m-Co_3O_4 and (b) c-Co_3O_4 pretreated; (c) m-Co_3O_4; and (d) c-Co_3O_4 reacted.

evidenced by XRD data (Figure 2a). At the 573 K reduction temperature, Co_3O_4 is partially reduced to CoO and Co, which leads to the catalyst being active at much lower temperatures as well as to high CO_2 conversion values (Figures 2a and 3a).

https://dx.doi.org/10.1021/acs.jpcc.0c09717
J. Phys. Chem. C 2021, 125, 7130−7141

However, a higher reduction temperature results in a decrease of m-Co_3O_4 catalytic activity, presumably because most of the CoO is over-reduced to metallic Co (Figures 2a and 3a). A similar trend is observed in the case of c-Co_3O_4. Here, with no reduction, the catalyst becomes active at higher temperatures compared to its reduced samples, for all of which CoO phase was registered (Figures 2b and 3b). A small amount of metallic Co appears during 573 K reduction, thus slightly increasing the catalytic performance of the catalyst.

In the CO_2 hydrogenation reaction, the major product was CH_4 with a minor amount of CO and ethane. At 573 K, the methane selectivity significantly increases up to 99% for m-Co_3O_4 reduced at 573 K, while for c-Co_3O_4, it is relatively the same—around 95% for all of the pretreatment conditions at this temperature (Figure 3c).

After being reused up to 4 times, the catalysts showed a small decrease in activity with every repeated cycle, which indicates that both catalysts have good operational stability. The decrease in the CO_2 conversion was more significant in the case of c-Co_3O_4 (Figure S2).

Albeit it is widely accepted that the active phase for CO_2 + H_2 reaction in Co-based systems is metallic Co;[16] in our case, Co_3O_4 catalysts reduced at the highest reduction temperature did not show the best activity; hence, the role of oxide phase cannot be ruled out. Thus, the better catalytic activity of m-Co_3O_4 can be ascribed to the enhanced basicity, which improves the adsorption and the activation of CO_2.

In general, a minimum reduction temperature of 573 K is required to activate m-Co_3O_4, while c-Co_3O_4 is active at 473 K reduction. The optimal reduction temperature that leads to better activity and higher methane selectivity is 573 K for both Co_3O_4s.

3.3. Co_3O_4 Catalysts Reduced at 573 K under CO_2 Methanation. *3.3.1. Oxidation States of Cobalt in Co_3O_4 Catalysts.* Commercial and mesoporous Co_3O_4 samples reduced at 573 K were investigated in more detail by means of X-ray photoelectron spectroscopy (XPS) to get information about the chemical state of surface cobalt species. For the oxidation-state analysis, the Co 2p high-resolution spectrum region was collected, where only the $2p_{3/2}$ part of the doublet was fitted. Peaks corresponding to Co^0 were fitted with an asymmetric peak shape of Lorentzian Asymmetric LA-(1.2,5,5).[21] For nonmetallic forms, a Gaussian−Lorentzian product function GL(30) peak shape was used. In the samples where Co^{2+} was present, a well observable satellite peak is present. For both the samples, the collected spectra are shown in Figure 4. The c-Co_3O_4 is more easily reduced by the pretreatment process; thus, more metallic Co is present on the surface compared to m-Co_3O_4, which aligns well with XRD results. c-Co_3O_4 is further reduced to metallic Co during the reaction (Figure 4b,d). The m-Co_3O_4, on the contrary, contains mainly Co^{2+} in the form of CoO and Co^{3+} is still present in the sample after reaction (Figure 4a,c). The distribution of various Co oxidation states was calculated based on the corresponding peak areas; the results are summarized in Table 2.

3.3.2. Surface Species Formed during CO_2 Methanation. For catalytic reactions, the exploration of surface species formed during the catalytic processes plays a decisive role in the understanding of the reaction mechanism. Toward this goal, DRIFT spectra were monitored at elevated temperatures in the presence of the reactant mixture/products. The assignment of IR bands and the detailed description are based on the vibrational fingerprints of relevant surface species, which were reported in previous publications.[22−26] It should be considered that the denoted wavenumbers may vary by ±5 cm^{-1} within one dataset as a function of temperature.

Table 2. Oxidation State of Cobalt for m-Co_3O_4 and c-Co_3O_4 after Pretreatment and after Reaction

	oxidation states			
	Co(0) (%)	Co(II) (%)	Co(III) (%)	total (%)
m-Co_3O_4 pretreated	34.20	48.10	17.70	100
m-Co_3O_4 reacted	24.81	68.80	6.39	100
c-Co_3O_4 pretreated	46.67	54.33	0.00	100
c-Co_3O_4 reacted	100.00	0.00	0.00	100

A series of IR spectra recorded during the CO_2 hydrogenation reaction for m-Co_3O_4 and c-Co_3O_4 are given in Figure 5. The observed bands and species formed in CO_2 hydrogenation are collected in Table S3.

In the spectra of m-Co_3O_4, various species were detected as the result of CO_2 adsorption on the surface of the catalyst (Figure 5a). CO_2 adsorption is favored by the presence of abundant basic sites, revealed from CO_2-TPD results. In DRIFTS spectra, this is evident from a strong-band gas-phase CO_2 at 2400−2200 cm^{-1} (not shown) and two strong twin-bands observed in the range of 3750−3550 cm^{-1}, which correspond to the combined tones of gas and adsorbed CO_2 molecules.[27]

The reaction is initiated at 473 K, evidenced by the appearance of the gas-phase methane at 1305 cm^{-1}. The corresponding methane feature can be detected at 3016 cm^{-1} as well. These gas-phase methane spectra are easily detectable during dry reforming of alcohols and CO_2 hydrogenation reactions.[28,29] To precisely assign other observed peaks corresponding to the possible reaction intermediates, CO_2 and formic acid (HCOOH) were adsorbed on the surface of m-Co_3O_4 (Figure 5a, inset). Carbon dioxide adsorbs with the formation of carboxylate (1623 and 1285 cm^{-1})[22,30] and bidentate carbonate (1542 and 1358 cm^{-1}) species.[22] The assignment of formate species was performed based on formic acid adsorption, which at 473 K resulted in peaks at 2866 (CH stretching frequency), 1573, and 1365 cm^{-1} (asymmetric and symmetric (O−C−O) stretching vibrations) (Figure 5a, inset).

During CO_2 + H_2 reaction, at low temperatures (up to 373 K), vibrational modes of carboxylate species at 1631 (ν_3(O−C−O)$_a$) and 1298 cm^{-1} (ν_3(O−C−O)$_s$) were detectable, which after 423 K shifted to 1653 and 1245 cm^{-1}, respectively. The peak at 1213 cm^{-1} could be assigned to bicarbonate adsorbed species that usually arise as a result of the interaction between CO_2 and the surface hydroxyl.[22,31] Carbonate bands are observed in the spectra (Figure 5a) at 1484 and 1342 cm^{-1} and may correspond to the ν_3(O−C−O)$_a$ and ν_3(O−C−O)$_s$ vibrations of polydentate carbonate.[30] From 423 K, bicarbonate species are converted to formate species at 2838, 1576, and 1381 cm^{-1}.

In the case of c-Co_3O_4 catalyst, the reaction starts with the formation of CH_4 at 473 K evidenced by the peaks at 1305 and 3016 cm^{-1}, which is in harmony with catalytic measurements (Figure 5b). Interestingly, the DRIFT spectra do not show any intermediates with significant concentrations up to this temperature. The infrared vibration bands at 1652 and 1267 cm^{-1} from 473 K are similar to those formed on m-Co_3O_4 and assigned to the adsorbed carboxylate species.[22] In addition to the carboxylate, carbonate peaks are present in the spectra

https://dx.doi.org/10.1021/acs.jpcc.0c09717
J. Phys. Chem. C 2021, 125, 7130−7141

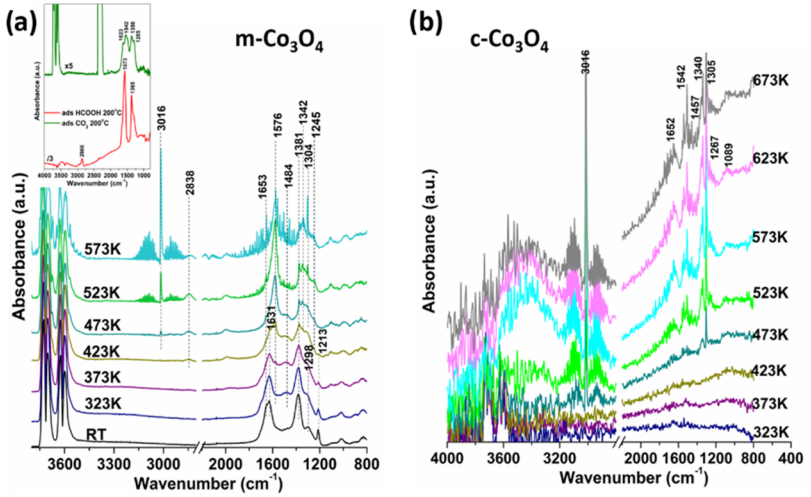

Figure 5. DRIFTS spectra of (a) m-Co_3O_4 and (b) c-Co_3O_4 obtained during CO_2 hydrogenation. Inset: CO_2 and HCOOH adsorption on m-Co_3O_4 at 473 K.

(Figure 5b) as broad overlapping bands observed in the spectral region from ~1300 to 1600 cm^{-1}. These are registered at 1457, 1361, and 1089 cm^{-1}, as well as ~1542 and 1340 cm^{-1}, which are ascribed to polydentate and bidentate forms of adsorbed carbonate, respectively.[22,32,33] These bands were also distinguished in the case of NiO[29] and Au/TiO_2[32] during the interaction of the $CO_2 + H_2$ mixture at low temperatures. In addition, broad physisorbed water peaks are detectable in the case of c-Co_3O_4 due to OH stretching vibration located at 3200−3600 cm^{-1}.[30]

On both the catalysts, carboxylate- and carbonate-like species were formed. Under the flow of hydrogen, the carboxylate (HOCO) can be converted to methane via the RWGS pathways[34]

$$HOCO_{(a)} \rightarrow CO_{(a)} + OH_{(a)} \quad (1)$$

$$CO_{(a)} + H_{(a)} \rightarrow HCO_{(a)} \quad (2)$$

In the following steps, HCO is hydrogenated further through the formation of perturbed CO

$$HCO_{(a)} + H_{(a)} \rightarrow H_2CO_{(a)} + 2H_{(a)} \rightarrow H_3C_{(a)} + OH_{(a)} \quad (3)$$

$$H_3C_{(a)} + H_{(a)} \rightarrow CH_{4(g)} \quad (4)$$

The RWGS mechanism is additionally supported by the small-intensity linearly adsorbed CO peak at 2076 cm^{-1} in the case of m-Co_3O_4. It is very "hot" (thermally excited) and has a transient existence; thus, a small fraction leaves the surface immediately or gets hydrogenated further.[35] Since this peak is observable even at room temperature, it should be considered that the $HOCO_{(a)}$ dissociation (step 1) occurs to a very limited extent at this low temperature. On the other hand, a very small amount of CO_2 may undergo dissociative adsorption on m-Co_3O_4 as well

$$CO_{2(g)} \rightarrow CO_{(a)} + O_{(a)} \quad (5)$$

After direct C−O bond cleavage in adsorbed CO, the subsequent carbon hydrogenation pathway cannot be eliminated as it was proposed in the study of CO dissociation on cobalt Fischer−Tropsch catalyst[36]

$$CO_{(a)} \rightarrow C_{(a)} + H_{(a)} \rightarrow CH_{4(a)} \rightarrow CH_{4(g)} \quad (6)$$

The intensity of CO is rather small. Its dissociation on metallic Co and carbon enrichment at the surface layer were not detected by XPS in our case. Despite this fact, the hydrogenation of subsurface carbon to some extent cannot be ruled out. The carbon formation and its penetration to the subsurface layer from the dissociation of CO in Co-based systems were observed and discussed.[37−39] It was determined that the hydrogenation step of carbon was slower than the C−O bond breaking.[36] Evidently, CO is very unstable with a short lifetime on c-Co_3O_4 since the corresponding peak is undetectable in the case of c-Co_3O_4.

Along with carboxylate and carbonates, formate species were registered on the m-Co_3O_4 while on the c-Co_3O_4, those species were undetectable. The formate species are identified as an important intermediate in CO_2 methanation-related works.[23,29,31,34,35,40−44] The formate species can be hydrogenated to hydrocarbons

$$HCOO_{(a)} \rightarrow H_2COH_{(a)} \rightarrow H_2C_{(a)} + OH_{(a)} \quad (7)$$

$$H_2C_{(a)} + 2H_{(a)} \rightarrow CH_{4(g)} \quad (8)$$

Furthermore, a broad peak at 1998 cm^{-1} is identified from 423 K on m-Co_3O_4. This band most likely belongs to the bridge bonded or hydrogen-perturbed CO species, which could originate from carboxylate or formate species.[29,34,45]

At high temperatures, CO selectivity is distinguished for both catalysts. $CO_{(gas)}$ product may emerge from the decomposition of carboxylate or formate (eqs 1 and 7)

$$HCOO_{(a)} \rightarrow CO_{(a)} + OH_{(a)} \quad (9)$$

This reaction step (eq 7) was considered recently in $CO_2 + H_2$ reaction in several cases, for example, on NiO, Pt/NiO,[29] Ru/Al_2O_3,[23] Au/TiO_2,[32] and Co/MnO_x.[45] Furthermore, formate produced by adsorption of HCOOH on metals,[46] oxides, and supported metal catalysts[41,42] decomposes to CO and CO_2.

It is also interesting that the adsorbed OH vibrations around 3200−3600 cm^{-1} were not registered on m-Co_3O_4. In this case, the recombination of OH groups to form water is assumed to happen very fast

$$nOH_{(a)} \rightarrow H_2O_{(g)} \quad (10)$$

https://dx.doi.org/10.1021/acs.jpcc.0c09717
J. Phys. Chem. C 2021, 125, 7130−7141

Tentatively, at least to some extent the higher catalytic activity of m-Co_3O_4 may be ascribed to the fact that formate species additionally contribute to the methane formation. It is strongly suggested that the formate forms at the Co/cobalt oxide interface. Supposedly, hydrogen atoms are created on metallic Co and they further migrate to the metal−support interface to react with the formate producing methane. In an attempt to prove that formate species observed on m-Co_3O_4 catalyst are not just a spectator but indeed a reaction intermediate, further DRIFTS spectra were collected (Figure 6).

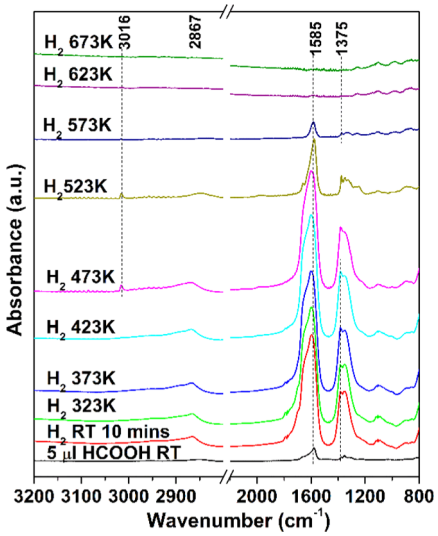

Figure 6. DRIFTS spectra of HCOOH adsorbed on m-Co_3O_4 and heated in H_2 to 673 K.

In this experiment, a small amount of formic acid was adsorbed on the m-Co_3O_4, after which mainly formate species were registered at 2867, 1585, and 1375 cm^{-1}. A similar spectral feature was obtained on the titania surface after HCOOH adsorption.[41,42] Formate species were thereafter heated under the flow of hydrogen. From 473 K, characteristic methane vibration at 3016 cm^{-1} with small intensity is detectable. Discussing the role of formate as an intermediate, it should be mentioned that formate is able to migrate from the metal/metal oxide interphase and accumulate on the oxide surface as in the case of the Ru/Al_2O_3 system.[47] Migrated formate species are therefore inactive and cannot be converted to produce CH_4. The migration starts from the interface, and the formate localizes on the cobalt oxide phase as an inactive spectator. To support this finding, a fully oxidized m-Co_3O_4 catalyst consisting of only the Co_3O_4 cubic spinel phase was tested in CO_2 methanation under identical conditions. In that case, formate species were registered, but no methane was formed. Thus, formate is proven to be an active intermediate resulting in the formation of CH_4; however, the carboxylate route cannot be excluded.

3.3.3. Insight into Structural Defects with X-ray Photoelectron and Raman Spectroscopy. The most prevailing structural defects in the Co_3O_4 system are accepted to be the oxygen vacancies.[48] They are formed during the reduction of higher valent metal ions (Ti^{4+}, W^{6+}, Co^{3+}) to lower-valent metal ions (Ti^{3+}, W^{5+}, Co^{2+}).[49] The characterization of oxygen vacancies was carried out by means of Raman and X-ray photoelectron spectroscopy techniques (Figure 7).

As described earlier, pure Co_3O_4 has five Raman-activated modes, 194, 482, 522, 618, and 691 cm^{-1} attributed to the F_{2g}, E_g, F_{2g}, and A_{1g} phonon modes.[50] Among them, the band at ∼194 cm^{-1} is characteristic for tetrahedral sites and can be ascribed to the vibration of $Co^{2+}-O^{2-}$ while that at ∼690 cm^{-1} is characteristic for octahedral sites and therefore corresponds to the Raman vibration of $Co^{3+}-O^{2-}$.[51] As shown in Figure 7a, on the m-Co_3O_4 sample, before pretreatment, $Co^{2+}-O^{2-}$ and $Co^{3+}-O^{2-}$ are observed at 193.5 and 688.5 cm^{-1}, respectively. After pretreatment, these Raman bands almost completely match those before pretreatment, which points at minuscule structural defects in the m-Co_3O_4. In the case of c-Co_3O_4 (Figure 7b), a considerable shift to higher frequencies for the bands corresponding to $Co^{2+}-O^{2-}$ and $Co^{3+}-O^{2-}$ vibrations is observed. This blueshift of the Raman bands can be attributed to the photon-confinement effects of the surface oxygen vacancies.[52] Moreover, after pretreatment on c-Co_3O_4, the Raman band at 528 cm^{-1} intensifies and becomes significantly broader. This is assigned to the defect-induced Raman peak arising from the one-phonon density of states scattering on CoO.[53]

The predominance of oxygen vacancies in c-Co_3O_4 compared to m-Co_3O_4 was further supported by XPS of the Co_3O_4 catalysts after pretreatment. As seen from Figure 7c,d, two kinds of oxygen species are fitted in O 1s spectra. The peak at ∼529.1 eV is assigned to lattice oxygen species (O_{latt}), whereas the one located at ∼530.8 eV corresponds to the surface adsorbed oxygen (O_{ads}).[54] The number of surface oxygen vacancies can be understood in terms of the O_{ads}/O_{latt} ratio. The higher ratio reveals more surface oxygen vacancies having formed. Judging from the O_{ads}/O_{latt} ratios calculated on the basis of peak areas in the deconvoluted spectra (Figure 7c,d), it is evident that c-Co_3O_4 is more abundant with surface oxygen vacancies compared to m-Co_3O_4. These results are consistent with Raman data.

3.3.4. Characterization of Spent Catalysts. The crystal structure of Co_3O_4 catalysts was recorded for the spent catalysts (Figure 8). In the case of m-Co_3O_4, apart from CoO (reflections at 2θ = 36.8, 42.5°), a mixture of metallic Co phases formed, in which peaks at 2θ = 44.6, 51.8, and 76.1° indicate the presence of fcc Co along with peaks at 2θ = 47.8, 76.1° corresponding to the hcp phase. c-Co_3O_4 lacks any peaks of cobalt oxidized forms and is present almost exclusively in the form of hcp metallic Co (2θ = 41.7, 44.7, 47.6, and 76.1°) (JSPDC card no. 05-0727).[55] The broad peak around 2θ = 26° is attributed to graphitic carbon that appears in all spent Co-based catalysts.[39]

X-ray structures of both catalysts after pretreatment at 573 K were also compared. This time, the patterns were registered at a slower scan rate to identify all of the components, and under inert atmosphere (N_2) to avoid reoxidation (Figure S3a).

In Figure S3a, m-Co_3O_4 after pretreatment shows a peak at 2θ = 38.4 and 78.2° corresponding to Co_3O_4 cubic spinel structure. Also, some reflections of CoO are detectable at 2θ = 36.6 and 42.6°. The rest of the peaks denotes the presence of metallic Co. The peaks at 44.5 and 75.6° were assigned to the cobalt fcc crystal structure. The peak at 47.7° was attributed to metallic Co in the hcp phase. For c-Co_3O_4, reflection at 38.4° belongs to Co_3O_4, while those at 41.7, 44.6, and 47.6° correspond to the hcp phase of Co. Reflection with a small intensity at 51.5° is characteristic for fcc Co, and the peak at 76° can be assigned to both fcc and hcp Co.[55] Altogether, it can be seen that after pretreatment, cobalt on m-Co_3O_4 is

https://dx.doi.org/10.1021/acs.jpcc.0c09717
J. Phys. Chem. C 2021, 125, 7130−7141

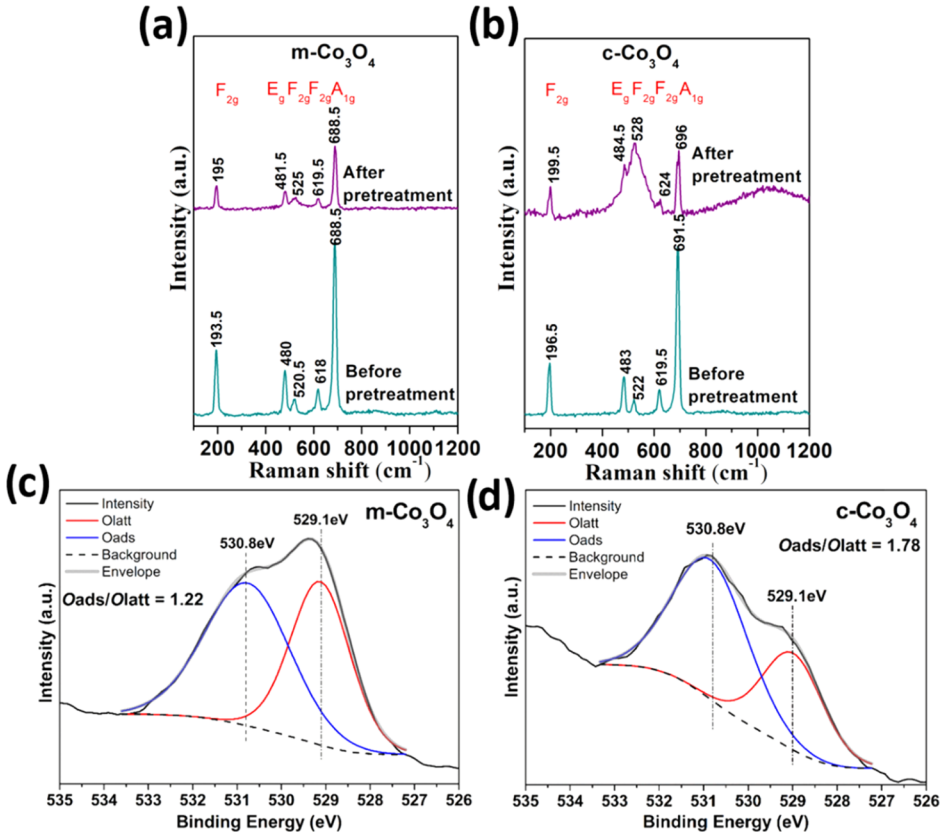

Figure 7. Raman spectra of (a) m-Co_3O_4 and (b) c-Co_3O_4; XPS O 1s spectra of (c) m-Co_3O_4 and (d) c-Co_3O_4.

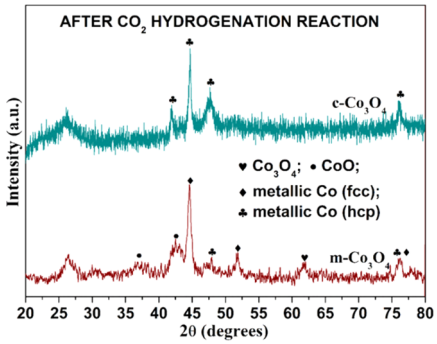

Figure 8. XRD patterns of m-Co_3O_4 and c-Co_3O_4 after CO_2 + H_2 reaction.

primarily in the fcc phase while on c-Co_3O_4, the hcp phase dominates.

Thus, XRD results showed that after pretreatment, there is a mixture of Co phases observed in the catalysts, and in the case of c-Co_3O_4, a phase transition from Co-fcc to Co-hcp occurs more readily. It was reported by several scholars that the Co-fcc/Co-hcp phase transition takes place as a result of in situ irreversible transformation of Co_2C to Co (hcp) under CO rich atmosphere as during the CO oxidation reaction.[56,57] The formation of carbides was proposed in the CO_2 + H_2 reaction as well.[58] However, in the present experiment, carbides were detected neither in XRD (Figure 8) nor in the XPS C 1s region of the spent catalysts. It may be suggested that the transformation of Co(fcc)−Co_2C−Co(hcp) happens fast enough to be detected. To ascertain or disprove the formation of cobalt carbide, CO_2 + H_2 reaction was performed on the c-Co_3O_4 catalyst, but the flow of CO_2 was eliminated, that is, the catalyst was pretreated and heated in H_2 under reaction conditions. The recorded XRD pattern (Figure S3b) demonstrates that the c-Co_3O_4 catalyst after reaction with H_2 and the one after CO_2 methanation reaction have the same XRD peaks, associated with mainly Co(hcp) phase structure. This suggests that the Co fcc−hcp phase transition is not caused by the CO_2 hydrogenation reaction; hence, the possibility of Co_2C formation under our reaction conditions and its influence on the mechanism were eliminated. What really causes the phase transition is hydrogenation in the temperature range of 473−673 K. The hydrogenation process is commonly known to induce the accumulation of structural defects.[49,59] It is proposed that the Co-fcc/Co-hcp phase shift could be facilitated in the case of c-Co_3O_4 due to the less ordered crystal structure and abundant oxygen vacancies sites. Discussing the role of Co phases in CO_2 + H_2 reaction, it should be noted that Co(hcp) was theoretically and experimentally proven to be more active than a cubic phase in Fischer−Tropsch synthesis presumably due to more surface defects as active sites.[56,60] In this experiment, apparently, the hcp phase of metallic Co seems less catalytically active in CO_2 methanation reaction since c-Co_3O_4, despite having more metallic Co on the surface, shows poorer catalytic performance compared to its mesoporous counterpart. Intuitively, this phenomenon may be ascribed to the presence of a larger degree of sites needed for CO_2 methanation on m-Co_3O_4 (weak basic sites, crucial for CO_2 activation) rather than to the influence of the cobalt crystal phase.[61] A more precise explanation obviously requires more investigation, which is not in the scope of this work.

3.4. Effect of Platinum Nanoparticles Loading. This chapter is aimed to investigate the competitiveness of free-

https://dx.doi.org/10.1021/acs.jpcc.0c09717
J. Phys. Chem. C 2021, 125, 7130−7141

standing supports with noble-metal-loaded samples. As the reference experiment, 1% 5 nm-sized platinum particles were deposited onto the surface of m-Co_3O_4 and c-Co_3O_4 catalysts. The resulting catalysts were denoted as 1% 5 nm Pt/m-Co_3O_4 and 1% 5 nm Pt/c-Co_3O_4, respectively.

The catalytic performance of Pt nanoparticle-loaded catalysts was evaluated for CO_2 hydrogenation reaction under the same reaction conditions as for free-standing supports. The reduction temperature for all of the catalysts was 573 K. The product distribution was the same—CH_4 with a small amount of CO and minor ethane formation. The maximum CO_2 consumption rates as well as the selectivity of Pt/supported catalysts compared to free-standing supports are summarized in Table 3. Decorating m-Co_3O_4 with 1% 5 nm Pt

Table 3. Maximum CO_2 Consumption Rate Data for the Catalysts

catalysts	temperature (K)	maximum CO_2 consumption rate ($nmol \cdot g^{-1} \cdot s^{-1}$)	CH_4 selectivity (%)	CO selectivity (%)
m-Co_3O_4	583	17 180	99.1	0.8
c-Co_3O_4	583	12 767	95.8	2.4
1% Pt/m-Co_3O_4	612	23 465	95.7	4.2
1% Pt/c-Co_3O_4	640	21 811	94.0	5.6

nanoparticles resulted in enhanced activity by a factor of 1.3 at the maximum. The promoting effect was more pronounced in the case of c-Co_3O_4 (by 1.8 times).

The higher catalytic activity for 1% 5 nm Pt/m-Co_3O_4 compared to 1% 5 nm Pt/c-Co_3O_4 catalyst can be attributed to the presence of uniform-sized completely separated 5 nm Pt nanoparticles inside the mesopores of Co_3O_4. The enhancement effect of Pt nanoparticles can arise from providing new active centers at the Pt/support interphase that are mainly responsible for CO formation.[35,62] Therefore, CH_4 selectivity drops to lower values in Pt-loaded catalysts compared to free-standing supports (Table 3). Another factor that could result in promoting catalytic activity is the H_2-spillover effect on Pt atoms,[63,64] since the C−O bond cleavage is known to be assisted by hydrogen.[65]

3.5. Discussion of the CO_2 Methanation Reaction Mechanism. Even though metallic Co is commonly acknowledged to serve as the active site in CO_2 methanation reaction for Co-based catalysts,[10,11,16,66] the results reported in this work support that for CO_2 methanation, both cobalt oxide phase and metallic phase are important. This is confirmed by catalytic experiments, from which the catalysts reduced at the highest temperature—having more metallic Co—did not demonstrate the best performance. It is believed that for Co_3O_4 systems in this work, cobalt oxide phase is mainly responsible for CO_2 activation while dissociation of H_2 happens on metallic Co.[45] For m-Co_3O_4, CO_2 activation is promoted by abundant weak basic sites,[13] while in the case of c-Co_3O_4, it occurs due to the presence of oxygen vacancies confined in cobalt oxide lattice structure.[48]

Apart from carboxylate species formed as the result of associative adsorption and subsequent hydrogenation on both Co_3O_4s, the formate intermediate additionally appears in the case of m-Co_3O_4, which was confirmed to contribute to the overall methane formation. It is strongly suggested that the formation of reaction intermediates—carboxylate and formate—takes place on the Co/cobalt oxide interphase as it was proposed for Co/manganese oxide systems.[45] Thus, the 573 K reduction temperature results in faster catalyst activation as well as in higher CH_4 selectivity because of the formation of optimal composite interphase—Co/cobalt oxide. The catalyst properties−performance correlations in the CO_2 methanation reaction for the catalysts in question are summarized in Figure 9. In the illustration, it is highlighted that carboxylate

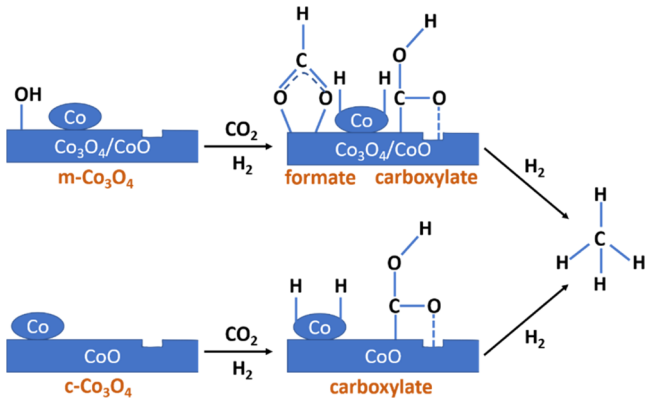

Figure 9. Catalyst properties−performance correlations in CO_2 methanation reaction in Co_3O_4 systems.

intermediate is stabilized by the oxygen vacancies present in both the Co_3O_4 systems but dominating on the c-Co_3O_4.[67] Additionally, the CO_2 molecules are activated on weak basic sites located exclusively on the m-Co_3O_4 by producing bicarbonate species, which are subsequently transformed to formate intermediate.

At high reaction temperatures, the CO selectivity considerably increases for both the catalysts, arising from the decomposition of carboxylate or formate species. XPS findings revealed that after the CO_2 + H_2 reaction, c-Co_3O_4 is totally reduced and m-Co_3O_4 is mostly oxidized. Oxidation of m-Co_3O_4 may be the result of an accumulation of formate species on the oxide surface.[42] To some extent, oxidation may be attributed to the water molecules formed during the reaction,[68] but since the DRIFTS spectra of m-Co_3O_4 do not show any significant concentration of adsorbed OH during the whole temperature range, this contribution is considered minor. On the other hand, c-Co_3O_4 does not have accumulated formate species on the surface; therefore, it is almost fully reduced by the constant excess of H_2 present in the reaction mixture. Although some authors could not reach complete reduction for Co-based systems even at high temperatures,[17] for this system, it was shown that c-Co_3O_4 is very prone to reduction and can be fully reduced under reaction conditions (Figure 3Sb).

Concerning the deactivation of the catalysts, the deposition of carbon through the direct dissociation of CO is accepted as the main reason.[39] It should be noted that for m-Co_3O_4, deactivation is much slower than for c-Co_3O_4. The limitation of coke formation on m-Co_3O_4 can be ascribed to the stronger surface basicity of the catalyst.[13] The fast deactivation of c-Co_3O_4 may originate from the fast reduction and unavailability of the cobalt oxide phase for CO_2 activation. Another reason could lie in the crystal structure of metallic Co. It is possible that the hcp phase prevailing on c-Co_3O_4 has poorer catalytic activity than the cubic one in CO_2 methanation, but claiming this would require more structural investigation.

https://dx.doi.org/10.1021/acs.jpcc.0c09717
J. Phys. Chem. C 2021, 125, 7130−7141

4. CONCLUSIONS

As a final remark, it is important to emphasize that Co_3O_4 is a complex dynamic system whose performance in CO_2 methanation reaction is extremely structure-sensitive (Table S1). Despite being the same material, the bulk and surface properties of both Co_3O_4s (such as morphology, cobalt oxidation states, acid−base properties, presence of defect sites) were quite different, which directly influences the catalytic capability and the reaction mechanism.

Both metallic cobalt and cobalt oxide phases are participating in the activation of the reactants and the stabilization of the intermediates. Metallic Co activates the hydrogen molecules while activation of CO_2 takes place on the cobalt oxide phase. The carbon dioxide activation may also occur on metallic Co in the case of dissociative CO_2 adsorption. Two kinds of active reaction intermediates were detected—carboxylate and formate. Oxygen vacancies prevailing on the c-Co_3O_4 serve as the sites for CO_2 adsorption to produce carboxylate species. Weak basic sites detected exclusively on m-Co_3O_4 promote the CO_2 activation and result in the formate intermediate. There is a possibility that a certain part of the formate migrates from the interface to the oxide phase and accumulates there as an inactive spectator. The CO_2 methanation intermediates are proposed to form at the Co/cobalt oxide interface. The formation of carbon is regarded as the main cause for the deactivation of the catalysts and originates from the CO dissociation at metallic Co sites.

The results of the present study proved that m-Co_3O_4 is a cheap, noble-metal-free catalyst for CO_2 methanation with competitive activity and ∼100% CH_4 selectivity (Table S1). Results obtained in this work emphasize the importance of morphology as well as metal oxide states in the given catalytic process. Investigating the role of these species and tuning the morphology enables the design of new noble-metal-free catalytic systems for CO_2 methanation to reach high activity and methane selectivity.

■ ASSOCIATED CONTENT

Supporting Information

The Supporting Information is available free of charge at https://pubs.acs.org/doi/10.1021/acs.jpcc.0c09717.

> Comparison of different Co-based catalysts in CO_2 methanation, H_2-TPR data, maximum CO_2 consumption rate values, catalytic stability results, adsorbed species with their assigned IR bands, and XRD of catalysts after pretreatment (PDF)

■ AUTHOR INFORMATION

Corresponding Author

András Sápi − *Interdisciplinary Excellence Centre, Department of Applied and Environmental Chemistry, University of Szeged, H-6720 Szeged, Hungary;* orcid.org/0000-0001-6557-0731; Email: sapia@chem.u-szeged.hu

Authors

Anastasiia Efremova − *Interdisciplinary Excellence Centre, Department of Applied and Environmental Chemistry, University of Szeged, H-6720 Szeged, Hungary*

T. Rajkumar − *Interdisciplinary Excellence Centre, Department of Applied and Environmental Chemistry, University of Szeged, H-6720 Szeged, Hungary*

Ákos Szamosvölgyi − *Interdisciplinary Excellence Centre, Department of Applied and Environmental Chemistry, University of Szeged, H-6720 Szeged, Hungary*

Kornélia Baán − *Interdisciplinary Excellence Centre, Department of Applied and Environmental Chemistry, University of Szeged, H-6720 Szeged, Hungary*

Imre Szenti − *Interdisciplinary Excellence Centre, Department of Applied and Environmental Chemistry, University of Szeged, H-6720 Szeged, Hungary*

Juan Gómez-Pérez − *Interdisciplinary Excellence Centre, Department of Applied and Environmental Chemistry, University of Szeged, H-6720 Szeged, Hungary;* orcid.org/0000-0002-2736-2015

Gábor Varga − *Interdisciplinary Excellence Centre, Department of Applied and Environmental Chemistry, University of Szeged, H-6720 Szeged, Hungary; Materials and Solution Structure Research Group, Institute of Chemistry, University of Szeged, H-6720 Szeged, Hungary;* orcid.org/0000-0002-7131-1629

János Kiss − *Interdisciplinary Excellence Centre, Department of Applied and Environmental Chemistry, University of Szeged, H-6720 Szeged, Hungary; MTA-SZTE Reaction Kinetics and Surface Chemistry Research Group, H-6720 Szeged, Hungary*

Gyula Halasi − *Extreme Light Infrastructure-ALPS, ELI-HU Non-Profit Ltd., H-6720 Szeged, Hungary*

Ákos Kukovecz − *Interdisciplinary Excellence Centre, Department of Applied and Environmental Chemistry, University of Szeged, H-6720 Szeged, Hungary;* orcid.org/0000-0003-0716-9557

Zoltán Kónya − *Interdisciplinary Excellence Centre, Department of Applied and Environmental Chemistry, University of Szeged, H-6720 Szeged, Hungary; MTA-SZTE Reaction Kinetics and Surface Chemistry Research Group, H-6720 Szeged, Hungary;* orcid.org/0000-0002-9406-8596

Complete contact information is available at: https://pubs.acs.org/10.1021/acs.jpcc.0c09717

Notes

The authors declare no competing financial interest.

■ ACKNOWLEDGMENTS

A.S. gratefully acknowledges the support of the Bolyai Janos Research Fellowship of the Hungarian Academy of Sciences. A.S. and I.S. are grateful for "UNKP-20-5-SZTE-663" and "UNKP-20-4-SZTE-634", respectively for the New National Excellence Program of the Ministry for Innovation and Technology. The financial support of the Hungarian National Research, Development and Innovation Office through the GINOP-2.3.2-15-2016-00013 project "Intelligent materials based on functional surfaces - from syntheses to applications" and the Ministry of Human Capacities through the EFOP-3.6.1-16-2016-00014 project and the 20391-3/2018/FEKUSTRAT are acknowledged.

■ REFERENCES

(1) Wang, W.; Wang, S.; Ma, X.; Gong, J. Recent Advances in Catalytic Hydrogenation of Carbon Dioxide. *Chem. Soc. Rev.* **2011**, *40*, 3703−3727.

(2) Li, W.; Wang, H.; Jiang, X.; Zhu, J.; Liu, Z.; Guo, X.; Song, C. A Short Review of Recent Advances in CO_2 Hydrogenation to Hydrocarbons over Heterogeneous Catalysts. *RSC Adv.* **2018**, *8*, 7651−7669.

(3) Razali, N. A. M.; Lee, K. T.; Bhatia, S.; Mohamed, A. R. Heterogeneous Catalysts for Production of Chemicals Using Carbon Dioxide as Raw Material: A Review. *Renewable Sustainable Energy Rev.* **2012**, *16*, 4951−4964.
(4) Sakakura, T.; Choi, J.-C.; Yasuda, H. Transformation of Carbon Dioxide. *Chem. Rev.* **2007**, *107*, 2365−2387.
(5) Lou, Y.; Liu, J. CO Oxidation on Metal Oxide Supported Single Pt Atoms: The Role of the Support. *Ind. Eng. Chem. Res.* **2017**, *56*, 6916−6925.
(6) An, K.; Alayoglu, S.; Musselwhite, N.; Plamthottam, S.; Melaet, G.; Lindeman, A. E.; Somorjai, G. A. Enhanced CO Oxidation Rates at the Interface of Mesoporous Oxides and Pt Nanoparticles. *J. Am. Chem. Soc.* **2013**, *135*, 16689−16696.
(7) Xu, X.; Fu, Q.; Gan, L.; Zhu, J.; Bao, X. Interface-Confined FeOx Adlayers Induced by Metal Support Interaction in Pt/FeOx Catalysts. *J. Phys. Chem. B* **2018**, *122*, 984−990.
(8) Liu, X.; Liu, M.-H.; Luo, Y.-C.; Mou, C.-Y.; Lin, S. D.; Cheng, H.; Chen, J.-M.; Lee, J.-F.; Lin, T.-S. Strong Metal−Support Interactions between Gold Nanoparticles and ZnO Nanorods in CO Oxidation. *J. Am. Chem. Soc.* **2012**, *134*, 10251−10258.
(9) Bonanni, S.; Aït-Mansour, K.; Brune, H.; Harbich, W. Overcoming the Strong Metal− Support Interaction State: CO Oxidation on TiO_2 (110)-Supported Pt Nanoclusters. *ACS Catal.* **2011**, *1*, 385−389.
(10) Yang, C.; Liu, S.; Wang, Y.; Song, J.; Wang, G.; Wang, S.; Zhao, Z. J.; Mu, R.; Gong, J. The Interplay between Structure and Product Selectivity of CO2 Hydrogenation. *Angew. Chem.* **2019**, *131*, 11364−11369.
(11) Wang, L.; Guan, E.; Wang, Y.; Wang, L.; Gong, Z.; Cui, Y.; Meng, X.; Gates, B. C.; Xiao, F.-S. Silica Accelerates the Selective Hydrogenation of CO_2 to Methanol on Cobalt Catalysts. *Nat. Commun.* **2020**, *11*, No. 1033.
(12) Kleitz, F.; Choi, S. H.; Ryoo, R. Cubic Ia3 d Large Mesoporous Silica: Synthesis and Replication to Platinum Nanowires, Carbon Nanorods and Carbon Nanotubes. *Chem. Commun.* **2003**, 2136−2137.
(13) Pan, Q.; Peng, J.; Sun, T.; Wang, S.; Wang, S. Insight into the Reaction Route of CO_2 Methanation: Promotion Effect of Medium Basic Sites. *Catal. Commun.* **2014**, *45*, 74−78.
(14) Song, W.; Poyraz, A. S.; Meng, Y.; Ren, Z.; Chen, S.-Y.; Suib, S. L. Mesoporous Co_3O_4 with Controlled Porosity: Inverse Micelle Synthesis and High-Performance Catalytic CO Oxidation at −60 C. *Chem. Mater.* **2014**, *26*, 4629−4639.
(15) Wang, Y.; Zheng, K.; Hu, X.; Zhou, W.; Wei, X.; Zhao, Y. Y_2O_3 Promoted Co_3O_4 Catalyst for Catalytic Decomposition of N_2O. *Mol. Catal.* **2019**, *470*, 104−111.
(16) Ouyang, B.; Xiong, S.; Zhang, Y.; Liu, B.; Li, J. The Study of Morphology Effect of Pt/Co_3O_4 Catalysts for Higher Alcohol Synthesis from CO_2 Hydrogenation. *Appl. Catal., A* **2017**, *543*, 189−195.
(17) Horváth, É.; Baán, K.; Varga, E.; Oszkó, A.; Vágó, Á.; Törő, M.; Erdőhelyi, A. Dry Reforming of CH_4 on Co/Al_2O_3 Catalysts Reduced at Different Temperatures. *Catal. Today* **2017**, *281*, 233−240.
(18) Qiu, J.; Yu, M.; Zhang, Z.; Cai, X.; Guo, G. Synthesis of Co3O4/Nitrogen-Doped Carbon Composite from Metal-Organic Framework as Anode for Li-Ion Battery. *J. Alloys Compd.* **2019**, *775*, 366−371.
(19) Qin, H.; Lao, S.; Liu, Z.; Zhu, J.; Li, Z. Effects of Heat Treatment on the Structure, Morphology and Electrocatalytic Activity of Cobalt Hydroxide Electrocatalyst. *Int. J. Hydrogen Energy* **2010**, *35*, 1872−1878.
(20) Wang, D.; Guo, J.; Hu, D.; Xu, Q.; Zhang, L.; Wang, J. Co@Co_3O_4 Prepared in Situ from Metallic Co as an Efficient Semiconductor Catalyst for Photocatalytic Water Oxidation. *ACS Sustainable Chem. Eng.* **2018**, *6*, 8300−8307.
(21) Biesinger, M. C.; Payne, B. P.; Grosvenor, A. P.; Lau, L. W.; Gerson, A. R.; Smart, R. S. C. Resolving Surface Chemical States in XPS Analysis of First Row Transition Metals, Oxides and Hydroxides: Cr, Mn, Fe, Co and Ni. *Appl. Surf. Sci.* **2011**, *257*, 2717−2730.
(22) Baltrusaitis, J.; Schuttlefield, J.; Zeitler, E.; Grassian, V. H. Carbon Dioxide Adsorption on Oxide Nanoparticle Surfaces. *Chem. Eng. J.* **2011**, *170*, 471−481.
(23) Falbo, L.; Visconti, C. G.; Lietti, L.; Szanyi, J. The Effect of Co on CO_2 Methanation over Ru/Al_2O_3 Catalysts: A Combined Steady-State Reactivity and Transient DRIFT Spectroscopy Study. *Appl. Catal., B* **2019**, *256*, No. 117791.
(24) Su, C.; Suarez, D. L. In Situ Infrared Speciation of Adsorbed Carbonate on Aluminum and Iron Oxides. *Clays Clay Miner.* **1997**, *45*, 814−825.
(25) Chuang, C.-C.; Wu, W.-C.; Huang, M.-C.; Huang, I.-C.; Lin, J.-L. FTIR Study of Adsorption and Reactions of Methyl Formate on Powdered TiO_2. *J. Catal.* **1999**, *185*, 423−434.
(26) Zhao, K.; Wang, L.; Moioli, E.; Calizzi, M.; Züttel, A. Identifying Reaction Species by Evolutionary Fitting and Kinetic Analysis: An Example of CO_2 Hydrogenation in DRIFTS. *J. Phys. Chem. C* **2019**, *123*, 8785−8792.
(27) Wu, J. C.; Huang, C.-W. In Situ DRIFTS Study of Photocatalytic CO_2 Reduction under A Irradiation. *Front. Chem. Eng. China* **2010**, *4*, 120−126.
(28) Ferencz, Z.; Erdohelyi, A.; Baán, K.; Oszkó, A.; Óvári, L.; Kónya, Z.; Papp, C.; Steinrück, H.-P.; Kiss, J. Effects of Support and Rh Additive on Co-Based Catalysts in the Ethanol Steam Reforming Reaction. *ACS Catal.* **2014**, *4*, 1205−1218.
(29) Sápi, A.; Halasi, Gy.; Kiss, J.; Dobó, D. G.; Juhász, K. L.; Kolcsár, V. J.; Ferenc, Zs.; Vári, G.; Matolin, V.; Erdőhelyi, A.; et al. In Situ DRIFTS and NAP-XPS Exploration of the Complexity of CO_2 Hydrogenation over Size-Controlled Pt Nanoparticles Supported on Mesoporous NiO. *J. Phys. Chem. C* **2018**, *122*, 5553−5565.
(30) Lin, L.; Yao, S.; Liu, Z.; Zhang, F.; Li, N.; Vovchok, D.; Martínez-Arias, A.; Castañeda, R.; Lin, J.; Senanayake, S. D.; et al. In Situ Characterization of Cu/CeO_2 Nanocatalysts for CO_2 Hydrogenation: Morphological Effects of Nanostructured Ceria on the Catalytic Activity. *J. Phys. Chem. C* **2018**, *122*, 12934−12943.
(31) Wang, X.; Shi, H.; Kwak, J. H.; Szanyi, J. Mechanism of CO_2 Hydrogenation on Pd/Al_2O_3 Catalysts: Kinetics and Transient DRIFTS-MS Studies. *ACS Catal.* **2015**, *5*, 6337−6349.
(32) László, B.; Baán, K.; Ferencz, Z.; Galbács, G.; Oszkó, A.; Kónya, Z.; Kiss, J.; Erdőohelyi, A. Gold Size Effect in the Thermal-Induced Reaction of CO_2 and H_2 on Titania-and Titanate Nanotube-Supported Gold Catalysts. *J. Nanosci. Nanotechnol.* **2019**, *19*, 470−477.
(33) Su, W.; Zhang, J.; Feng, Z.; Chen, T.; Ying, P.; Li, C. Surface Phases of TiO_2 Nanoparticles Studied by UV Raman Spectroscopy and FT-IR Spectroscopy. *J. Phys. Chem. C* **2008**, *112*, 7710−7716.
(34) László, B.; Baán, K.; Oszkó, A.; Erdőhelyi, A.; Kiss, J.; Kónya, Z. Hydrogen Evolution in the Photocatalytic Reaction between Methane and Water in the Presence of CO_2 on Titanate and Titania Supported Rh and Au Catalysts. *Top. Catal.* **2018**, *61*, 875−888.
(35) Kattel, S.; Yan, B.; Chen, J. G.; Liu, P. CO_2 Hydrogenation on Pt, Pt/SiO_2 and Pt/TiO_2: Importance of Synergy between Pt and Oxide Support. *J. Catal.* **2016**, *343*, 115−126.
(36) Chen, W.; Zijlstra, B.; Filot, I. A.; Pestman, R.; Hensen, E. J. Mechanism of Carbon Monoxide Dissociation on a Cobalt Fischer−Tropsch Catalyst. *ChemCatChem* **2018**, *10*, 136−140.
(37) Zonnevylle, M.; Geerlings, J.; Van Santen, R. Conversion of Surface Carbidic to Subsurface Carbon on Cobalt (0001): A Theoretical Study. *Surf. Sci.* **1990**, *240*, 253−262.
(38) Ciobîcă, I.; Van Helden, P.; Van Santen, R. Stability and Effects of Carbon-Induced Surface Reconstructions in Cobalt Fischer−Tropsch Synthesis. *Surf. Sci.* **2016**, *653*, 82−87.
(39) Ahn, C.-I.; Koo, H. M.; Jin, M.; Kim, J. M.; Kim, T.; Suh, Y.-W.; Yoon, K. J.; Bae, J. W. Catalyst Deactivation by Carbon Formation During CO Hydrogenation to Hydrocarbons on Mesoporous Co_3O_4. *Microporous Mesoporous Mater.* **2014**, *188*, 196−202.
(40) Solymosi, F.; Erdőhelyi, A. Hydrogenation of CO_2 to CH_4 over Alumina-Supported Noble Metals. *J. Mol. Catal.* **1980**, *8*, 471−474.

https://dx.doi.org/10.1021/acs.jpcc.0c09717
J. Phys. Chem. C 2021, 125, 7130−7141

(41) Kecskés, T.; Raskó, J.; Kiss, J. FTIR and Mass Spectrometric Study of HCOOH Interaction with TiO_2 Supported Rh and Au Catalysts. *Appl. Catal., A* **2004**, *268*, 9−16.
(42) Raskó, J.; Kecskés, T.; Kiss, J. Formaldehyde Formation in the Interaction of HCOOH with Pt Supported on TiO_2. *J. Catal.* **2004**, *224*, 261−268.
(43) Raskó, J.; Kecskés, T.; Kiss, J. Adsorption and Reaction of Formaldehyde on TiO_2-Supported Rh Catalysts Studied by FTIR and Mass Spectrometry. *J. Catal.* **2004**, *226*, 183−191.
(44) László, B.; Baán, K.; Varga, E.; Oszkó, A.; Erdőhelyi, A.; Kónya, Z.; Kiss, J. Photo-Induced Reactions in the CO_2-Methane System on Titanate Nanotubes Modified with Au and Rh Nanoparticles. *Appl. Catal., B* **2016**, *199*, 473−484.
(45) Varga, G.; Sápi, A.; Varga, T.; Baán, K.; Szenti, I.; Halasi, G.; Mucsi, R.; Óvári, L.; Kiss, J.; Fogarassy, Z.; et al. Ambient Pressure CO_2 Hydrogenation over a Cobalt/Manganese-Oxide Nanostructured Interface: A Combined In Situ and Ex Situ Study. *J. Catal.* **2020**, *386*, 70−80.
(46) Solymosi, F.; Kiss, J.; Kovacs, I. Adsorption and Decomposition of Formic Acid on Potassium-Promoted Rhodium (111) Surfaces. *J. Phys. Chem. A* **1988**, *92*, 796−803.
(47) Zhao, K.; Wang, L.; Calizzi, M.; Moioli, E.; Züttel, A. In Situ Control of the Adsorption Species in CO_2 Hydrogenation: Determination of Intermediates and Byproducts. *J. Phys. Chem. C* **2018**, *122*, 20888−20893.
(48) Tong, Y.; Mao, H.; Xu, Y.; Liu, J. Oxygen Vacancies Confined in Co_3O_4 Quantum Dots for Promoting Oxygen Evolution Electrocatalysis. *Inorg. Chem. Front.* **2019**, *6*, 2055−2060.
(49) Chen, H.; Yang, M.; Tao, S.; Chen, G. Oxygen Vacancy Enhanced Catalytic Activity of Reduced Co_3O_4 Towards P-Nitrophenol Reduction. *Appl. Catal., B* **2017**, *209*, 648−656.
(50) Hadjiev, V.; Iliev, M.; Vergilov, I. The Raman Spectra of Co_3O_4. *J. Phys. C: Solid State Phys.* **1988**, *21*, L199.
(51) Lou, Y.; Ma, J.; Cao, X.; Wang, L.; Dai, Q.; Zhao, Z.; Cai, Y.; Zhan, W.; Guo, Y.; Hu, P.; et al. Promoting Effects of In_2O_3 on Co_3O_4 for CO Oxidation: Tuning O_2 Activation and Co Adsorption Strength Simultaneously. *ACS Catal.* **2014**, *4*, 4143−4152.
(52) Wang, Z.; Wang, W.; Zhang, L.; Jiang, D. Surface Oxygen Vacancies on Co_3O_4 Mediated Catalytic Formaldehyde Oxidation at Room Temperature. *Catal. Sci. Technol.* **2016**, *6*, 3845−3853.
(53) Li, Y.; Qiu, W.; Qin, F.; Fang, H.; Hadjiev, V. G.; Litvinov, D.; Bao, J. Identification of Cobalt Oxides with Raman Scattering and Fourier Transform Infrared Spectroscopy. *J. Phys. Chem. C* **2016**, *120*, 4511−4516.
(54) Wang, X.; Li, X.; Mu, J.; Fan, S.; Chen, X.; Wang, L.; Yin, Z.; Tadé, M.; Liu, S. Oxygen Vacancy-Rich Porous Co_3O_4 Nanosheets toward Boosted NO Reduction by Co and Co Oxidation: Insights into the Structure−Activity Relationship and Performance Enhancement Mechanism. *ACS Appl. Mater. Interfaces* **2019**, *11*, 41988−41999.
(55) Ohtake, M.; Yabuhara, O.; Higuchi, J.; Futamoto, M. Preparation and Characterization of Co Single-Crystal Thin Films with hcp, fcc and bcc Structures. *J. Appl. Phys.* **2011**, *109*, No. 07C105.
(56) Kwak, G.; Woo, M. H.; Kang, S. C.; Park, H.-G.; Lee, Y.-J.; Jun, K.-W.; Ha, K.-S. In Situ Monitoring During the Transition of Cobalt Carbide to Metal State and Its Application as Fischer−Tropsch Catalyst in Slurry Phase. *J. Catal.* **2013**, *307*, 27−36.
(57) Sadeqzadeh, M.; Karaca, H.; Safonova, O.; Fongarland, P.; Chambrey, S.; Roussel, P.; Griboval-Constant, A.; Lacroix, M.; Curulla-Ferré, D.; Luck, F.; et al. Identification of the Active Species in the Working Alumina-Supported Cobalt Catalyst under Various Conditions of Fischer−Tropsch Synthesis. *Catal. Today* **2011**, *164*, 62−67.
(58) Kestel, U.; Fröhlich, G.; Borgmann, D.; Wedler, G. Hydrogenation of Carbon Dioxide on Cobalt Catalysts−Activation, Deactivation, Influence of Carbon Monoxide. *Chem. Eng. Technol.* **1994**, *17*, 390−396.
(59) Barzan, C.; Groppo, E.; Bordiga, S.; Zecchina, A. Defect Sites in H_2-Reduced TiO_2 Convert Ethylene to High Density Polyethylene without Activator. *ACS Catal.* **2014**, *4*, 986−989.
(60) Liu, J.-X.; Su, H.-Y.; Sun, D.-P.; Zhang, B.-Y.; Li, W.-X. Crystallographic Dependence of Co Activation on Cobalt Catalysts: Hcp Versus Fcc. *J. Am. Chem. Soc.* **2013**, *135*, 16284−16287.
(61) Bezemer, G. L.; Bitter, J. H.; Kuipers, H. P.; Oosterbeek, H.; Holewijn, J. E.; Xu, X.; Kapteijn, F.; van Dillen, A. J.; de Jong, K. P. Cobalt Particle Size Effects in the Fischer− Tropsch Reaction Studied with Carbon Nanofiber Supported Catalysts. *J. Am. Chem. Soc.* **2006**, *128*, 3956−3964.
(62) Sápi, A.; Kashaboina, U.; Ábrahámné, K. B.; Gómez-Pérez, J. F.; Szenti, I.; Halasi, G.; Kiss, J.; Nagy, B.; Varga, T.; Kukovecz, Á.; et al. Synergetic of Pt Nanoparticles and H-ZSM-5 Zeolites for Efficient CO_2 Activation: Role of Interfacial Sites in High Activity. *Front. Mater.* **2019**, *6*, 127.
(63) Spreafico, C.; Karim, W.; Ekinci, Y.; van Bokhoven, J. A.; VandeVondele, J. Hydrogen Adsorption on Nanosized Platinum and Dynamics of Spillover onto Alumina and Titania. *J. Phys. Chem. C* **2017**, *121*, 17862−17872.
(64) Zhang, J.; Gao, Z.; Wang, S.; Wang, G.; Gao, X.; Zhang, B.; Xing, S.; Zhao, S.; Qin, Y. Origin of Synergistic Effects in Bicomponent Cobalt Oxide-Platinum Catalysts for Selective Hydrogenation Reaction. *Nat. Commun.* **2019**, *10*, No. 4166.
(65) Shustorovich, E.; Bell, A. T. Analysis of CO Hydrogenation Pathways Using the Bond-Order-Conservation Method. *J. Catal.* **1988**, *113*, 341−352.
(66) Jimenez, J. D.; Wen, C.; Lauterbach, J. Design of Highly Active Cobalt Catalysts for CO_2 Hydrogenation Via the Tailoring of Surface Orientation of Nanostructures. *Catal. Sci. Technol.* **2019**, *9*, 1970−1978.
(67) Freund, H.-J.; Roberts, M. W. Surface Chemistry of Carbon Dioxide. *Surf. Sci. Rep.* **1996**, *25*, 225−273.
(68) Xu, L.; Ma, Y.; Zhang, Y.; Chen, B.; Wu, Z.; Jiang, Z.; Huang, W. Water Adsorption on a Co (0001) Surface. *J. Phys. Chem. C* **2010**, *114*, 17023−17029.

https://dx.doi.org/10.1021/acs.jpcc.0c09717
J. Phys. Chem. C 2021, 125, 7130−7141